Flexible Power Regulation and Limitation of Voltage Source Inverters under Unbalanced Grid Faults

Peng Cheng, *Member, IEEE*, Kongyuan Li, *Student Member, IEEE*, Chao Wu, *Member, IEEE*, Jing Ma, *Senior Member, IEEE*, and Limin Jia

***Abstract*—This paper develops a flexible power regulation and limitation strategy of voltage source inverters (VSIs) under unbalanced grid faults. When the classical power theory is used under unbalanced grid faults, the power oscillations and current distortions are inevitable. In the proposed strategy, the extended power theory is introduced to compute the power feedbacks together with the classical power theory. Based on the combination of the classical and extended power theory, the proposed strategy can achieve the sinusoidal current provision and the flexible regulation between three common targets, i.e., constant active power, balanced current, and constant reactive power. Meanwhile, the proposed strategy is associated with a power limiter, which is capable to keep the currents under the pre-defined threshold and to compute the maximum apparent power for better utilization of the inverter capacity. With this power limiter, the rated inverter capacity is fully used for both the active and reactive power provisions under unbalanced grid faults. Using the proposed power regulation and limitation, the VSI can avoid overcurrent tripping and flexibly regulate its power under unbalanced grid faults. All the conclusions are verified by the real-time hardware-in-loop tests.**

***Index Terms*—Flexible power regulation, Power limiter, Voltage source inverter, Unbalanced faults.**

I. INTRODUCTION

VOLTAGE SOURCE INVERTERS (VSIs) are widely used as the grid interface in the applications of renewable energy systems, distributed generation systems, and electrified transportation systems, where the dc power is converted to AC power. In practice, VSIs may operate with unbalanced voltages due to faults, low stiffness of the grid, unbalanced loads, etc [1]-[3]. In recent years, various controllers are designed on vector-orient control (VOC) and direct power control (DPC) to guarantee the enhanced operation with the unbalanced voltages.

Manuscript received April 29, 2021; revised September 22, 2021; accepted October 28, 2021. date of publication June 25, 2022; date of current version June 18, 2022.

This work is supported by the National Key Research and Development Program of China under Project 2021YFB2601600. (*Corresponding author: Peng Cheng.*)

Peng Cheng, Kongyuan Li, Jing Ma and Limin Jia are with the China Institute of Energy and Transportation Integrated Development, North China Electric Power University, Beijing, 102206, China (e-mail: p.cheng@ncepu.edu.cn; kongyuan_li@163.com; hdmajing@163.com; jialm@vip.sina.com).

Chao Wu is with the Department of Electrical Engineering, Shanghai Jiao Tong University, Shanghai 200240, China (e-mail: wuchao@sjtu.edu.cn)

Digital Object Identifier 10.30941/CESTEMS.2022.00021

A classical VOC for unbalanced issues based on rotating synchronization reference frame requires higher complex phase-locked loop (PLL) to synchronize with the grid [4]. Another classical VOC designed in the stationary reference frame may introduce more harmonics under unbalanced faults due to the current references based on instantaneous power theory [5], [6].

As an alternative approach, DPC has been studied to control the active and reactive power directly without the current control loop and PLL. A lookup-table DPC with hysteresis is initially designed and the switching signals are selected from a predefined switching table based on the signs of power errors and the position of the voltage vector. However, it produces substantial power ripples due to variable switching frequencies [7], [8]. Several improved DPC strategies are developed in [9]-[14]. In general, these strategies can be categorized into two groups. One is the model predictive control (MPC)-based DPC. MPC-DPC is developed with a cost function. By minimizing the cost function, multiple-vector-based MPC-DPC is developed with the constant switching frequency [9], [10]. But it is nonlinear and complicated to implement with additional computational burden. The other one is the space vector modulation (SVM)-based DPC, where the SVM is introduced to synthesize the voltage vector instead of the cost function and voltage vector selection in MPC-DPC. In [11], a proportional-integral plus resonant (PI+R) controller is developed in the improved DPC with the adjustable power compensations. However, the power compensations are calculated on the basis of the positive and negative sequence voltages and currents. Then, for removing the sequence extraction, an extended active and reactive power-based DPC is developed using the sliding mode control approach in [12]. However, the sliding mode controller is complicated to implement to guarantee the convergence to its equilibrium point. Recently, in [13], [14], a grid voltage modulated-DPC is proposed which can well track the power reference and maintain the highly sinusoidal current under balanced grid voltage conditions. But this method is only suitable for the balanced grid voltage, which restricts its application. Then, a negative-sequence parallel compensator is designed for guaranteeing balancing and sinusoidal stator currents in [15]. Further studies for achieving more control targets need to be conducted for unbalanced issues.

Under unbalanced grid voltage, the converter current may exceed its maximum value for tracking the prespecified

average power due to the decreased positive sequence voltage. Thus, a current/power limiter is essential to limit the currents at a predefined threshold for unbalanced voltages. In [16], a current limiter is designed on the basis of the current RMS values. In [17], an individual current limiter of each phase is proposed based on the current magnitude. In [18], the current magnitude of each phase is obtained based on the power factor and the voltage unbalance factor, while in [19], the instantaneous current of each phase is calculated with positive and negative sequence voltages. However, the complex calculation of the current RMS values and magnitude is needed with a higher computational burden.

It is mentioned in [20] that a limiter of the active and reactive powers instead of the currents is preferred in the renewable power generation. Meanwhile, a power limiter is designed to limit the power reference under unbalanced faults, but it is relevant to the phase angle between dual sequences and complex to implement. In [21], a new normal power, referring to the available converter rating under grid faults, is defined as the maximum power value according to the positive and negative sequence voltages under faults. The power limitation is simply given for one specific target under unbalanced faults.

Thus, the motivation of this paper is to develop a flexible power regulation and limitation of VSIs under unbalanced faults. Compared with the previous research, the power limiting method proposed in this paper can not only limit the current under the safety value, but also fully utilize the inverter capacity. Besides, the proposed method can provide a priority between the active and reactive power provisions, especially during grid faults. Under such case, according to the issued grid codes in [22],[23], the reactive power is usually set to be prior to the active power. With this method employed, the reactive power requirement can be firstly met, and then by fully utilization of the inverter capacity, the remain capacity is for the active power provision.

In this paper, by combining the classical and extended power theory, the flexible power feedbacks are detailly designed with an adjustable parameter, which establishes a trade-off between the current unbalance factor and twice grid frequency power oscillations. Then, a power limiter is proposed to limit the three phases converter currents under grid faults so as the converter remains connected to the rest of the grid. Meanwhile, the rated current is fully utilized for both the active and reactive power provisions under unbalanced faults when there is a priority between active power and reactive power. The paper is organized as follows. Section II gives the mathematic model of an inverter. In Section III, the feedback powers are flexibly designed with an adjustable parameter, and a flexible power limiter is developed. Then, the related results of the hardware-in-loop (HIL) tests are discussed in Section IV. Finally, Section V summarizes the conclusions.

II. Mathematic Model

A. Power Analysis

In this paper, the grid voltage is assumed to be simultaneously unbalanced but without regard to the zero-sequence component in a three-phase three-wire system. Thus, both the positive and negative sequence voltages/currents are expressed as,

$$\begin{cases} u_{g\alpha} = u_{g\alpha+} + u_{g\alpha-},\ u_{g\beta} = u_{g\beta+} + u_{g\beta-} \\ i_{\alpha} = i_{\alpha+} + i_{\alpha-},\ \ i_{\beta} = i_{\beta+} + i_{\beta-} \end{cases} \tag{1}$$

where subscripts +, − refer to the positive and negative sequence components,

$$\begin{cases} u_{g\alpha+} = U_{g+}\cos\left(\omega t + \theta_{u+}\right),\ u_{g\alpha-} = U_{g-}\cos\left(-\omega t + \theta_{u-}\right) \\ u_{g\beta+} = U_{g+}\sin\left(\omega t + \theta_{u+}\right),\ u_{g\beta-} = U_{g-}\sin\left(-\omega t + \theta_{u-}\right) \end{cases} \tag{2}$$

$$\begin{cases} i_{\alpha+} = I_{+}\cos\left(\omega t + \theta_{i+}\right), \quad i_{\beta+} = I_{+}\sin\left(\omega t + \theta_{i+}\right) \\ i_{\alpha-} = I_{-}\cos\left(-\omega t + \theta_{i-}\right),\ i_{\beta-} = I_{-}\sin\left(-\omega t + \theta_{i-}\right) \end{cases} \tag{3}$$

Based on the instantaneous power theory, the classical active and reactive power are calculated as,

$$\begin{cases} P_{cl} = 1.5\,\mathrm{Re}\left[u^{*}_{g\alpha\beta} i_{\alpha\beta}\right] = P_{cl0} + P_{cli2} + P_{clu2} \\ Q_{cl} = -1.5\,\mathrm{Im}\left[u^{*}_{g\alpha\beta} i_{\alpha\beta}\right] = Q_{cl0} + Q_{cli2} + Q_{clu2} \end{cases} \tag{4}$$

where "*" denotes the conjugate of the complex phasors,

$$\begin{cases} P_{cl0} = 1.5(u_{g\alpha+}i_{\alpha+} + u_{g\beta+}i_{\beta+} + u_{g\alpha-}i_{\alpha-} + u_{g\beta-}i_{\beta-}) \\ \quad = 1.5U_{g+}I_{+}\cos\left(\theta_{u+} - \theta_{i+}\right) + 1.5U_{g-}I_{-}\cos\left(\theta_{u-} - \theta_{i-}\right) \\ P_{cli2} = 1.5(u_{g\alpha+}i_{\alpha-} + u_{g\beta+}i_{\beta-}) = 1.5U_{g+}I_{-}\cos\left(2\omega t + \theta_{u+} - \theta_{i-}\right) \\ P_{clu2} = 1.5(u_{g\alpha-}i_{\alpha+} + u_{g\beta-}i_{\beta+}) = 1.5U_{g-}I_{+}\cos\left(-2\omega t + \theta_{u-} - \theta_{i+}\right) \end{cases} \tag{5}$$

$$\begin{cases} Q_{cl0} = 1.5(u_{g\beta+}i_{\alpha+} - u_{g\alpha+}i_{\beta+} + u_{g\beta-}i_{\alpha-} - u_{g\alpha-}i_{\beta-}) \\ \quad = 1.5U_{g+}I_{+}\sin\left(\theta_{u+} - \theta_{i+}\right) + 1.5U_{g-}I_{-}\sin\left(\theta_{u-} - \theta_{i-}\right) \\ Q_{cli2} = 1.5(u_{g\beta+}i_{\alpha-} - u_{g\alpha+}i_{\beta-}) = 1.5U_{g+}I_{-}\sin\left(2\omega t + \theta_{u+} - \theta_{i-}\right) \\ Q_{clu2} = 1.5(u_{g\beta-}i_{\alpha+} - u_{g\alpha-}i_{\beta+}) = 1.5U_{g-}I_{+}\sin\left(-2\omega t + \theta_{u-} - \theta_{i+}\right) \end{cases} \tag{6}$$

where U_{g+}, U_{g-} and I_{+}, I_{-} are the amplitudes of positive and negative sequence voltages and currents, θ_{u+}, θ_{u-} and θ_{i+}, θ_{i-} are the initial phase angle of positive and negative sequence voltages and currents, ω is the angular frequency of the grid voltage, respectively. The amplitudes of positive and negative sequence voltages are obtained with $T/4$ delayed signal cancellation method where T = 20 ms is the fundamental period.

Then, the extended active and reactive powers are calculated with a one-quarter-of-fundamental-period delayed voltage vector, corresponding to 90 electrical degrees which means that the voltage vector is simply delayed by $T/4$. The delayed α- and β-axis voltages are expressed as,

$$\begin{cases} u'_{g\alpha+} = U_{g+}\cos\left(\omega t + \theta_{u+} - \pi/2\right) = U_{g+}\sin\left(\omega t + \theta_{u+}\right) = u_{g\beta+} \\ u'_{g\beta+} = U_{g+}\sin\left(\omega t + \theta_{u+} - \pi/2\right) = -U_{g+}\cos\left(\omega t + \theta_{u+}\right) = -u_{g\alpha+} \\ u'_{g\alpha-} = U_{g-}\cos\left(-\omega t + \theta_{u-} + \pi/2\right) = -U_{g-}\sin\left(-\omega t + \theta_{u-}\right) = -u_{g\beta-} \\ u'_{g\beta-} = U_{g-}\sin\left(-\omega t + \theta_{u-} + \pi/2\right) = U_{g-}\cos\left(-\omega t + \theta_{u-}\right) = u_{g\alpha-} \end{cases} \tag{7}$$

where superscript ′ refers to the one-quarter-of-fundamental-period delayed vector.

The extended active and reactive powers are obtained by,

$$\begin{cases} P_{ex} = 1.5\,\mathrm{Im}\left[u'^{*}_{g\alpha\beta} i_{\alpha\beta}\right] = P_{ex0} + P_{exi2} + P_{exu2} \\ Q_{ex} = 1.5\,\mathrm{Re}\left[u'^{*}_{g\alpha\beta} i_{\alpha\beta}\right] = Q_{ex0} + Q_{exi2} + Q_{exu2} \end{cases} \tag{8}$$

where

$$\begin{cases} P_{ex0} = 1.5(u_{g\alpha+}i_{\alpha+} + u_{g\beta+}i_{\beta+} - u_{g\alpha-}i_{\alpha-} - u_{g\beta-}i_{\beta-}) \\ \quad = 1.5U_{g+}I_{+}\cos(\theta_{u+} - \theta_{i+}) - 1.5U_{g-}I_{-}\cos(\theta_{u-} - \theta_{i-}) \\ P_{exi2} = 1.5(u_{g\alpha+}i_{\alpha-} + u_{g\beta+}i_{\beta-}) = 1.5U_{g+}I_{-}\cos(2\omega t + \theta_{u+} - \theta_{i-}) \\ P_{exu2} = 1.5(-u_{g\alpha-}i_{\alpha+} - u_{g\beta-}i_{\beta+}) = -1.5U_{g-}I_{+}\cos(-2\omega t + \theta_{u-} - \theta_{i+}) \end{cases} \tag{9}$$

$$\begin{cases} Q_{ex0} = 1.5(u_{g\beta+}i_{\alpha+} - u_{g\alpha+}i_{\beta+} - u_{g\beta-}i_{\alpha-} + u_{g\alpha-}i_{\beta-}) \\ \quad = 1.5U_{g+}I_{+}\sin(\theta_{u+} - \theta_{i+}) - 1.5U_{g-}I_{-}\sin(\theta_{u-} - \theta_{i-}) \\ Q_{exi2} = 1.5(u_{g\beta+}i_{\alpha-} - u_{g\alpha+}i_{\beta-}) = 1.5U_{g+}I_{-}\sin(2\omega t + \theta_{u+} - \theta_{i-}) \\ Q_{exu2} = 1.5(u_{g\alpha-}i_{\beta+} - u_{g\beta-}i_{\alpha+}) = -1.5U_{g-}I_{+}\sin(-2\omega t + \theta_{u-} - \theta_{i+}) \end{cases} \tag{10}$$

As seen, the oscillating parts of classical and extended powers caused by negative sequence current and positive sequence voltage are equal, while those caused by positive sequence current and negative sequence voltage are opposite. As a result, equation (11) is obtained as,

$$\begin{cases} P_{cli2} = P_{exi2},\ P_{clu2} = -P_{exu2} \\ Q_{cli2} = Q_{exi2},\ Q_{clu2} = -Q_{exu2} \end{cases} \tag{11}$$

B. VSI Model

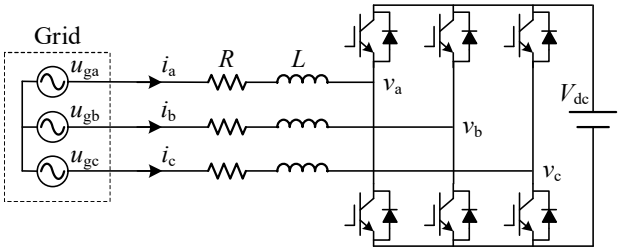

Fig. 1. Simplified circuit of voltage source inverter.

Fig. 1 gives a simplified circuit of a grid-connected VSI. Since dc-dc converter in PV application or a rectifier in wind application is connected to the dc side, a stiff dc source is assumed and then the dynamic of the dc input is not included. For simplified analysis, all the voltages and currents are per-unit values. Accordingly, the dynamics between VSI output voltage v, the grid voltages u and the output currents i in the stationary reference frame can be expressed as,

$$\begin{cases} L\dfrac{di_\alpha}{dt} = -Ri_\alpha - v_\alpha + u_{g\alpha} \\ L\dfrac{di_\beta}{dt} = -Ri_\beta - v_\beta + u_{g\beta} \end{cases} \tag{12}$$

where $v_{\alpha\beta}$, $i_{\alpha\beta}$ and $u_{g\alpha\beta}$ are the VSI output voltages, the output currents, and the grid voltages, L and R refer to the filter inductance and resistance, respectively.

The variations of active and reactive powers can be given as,

$$\begin{cases} \dfrac{dP_{cl}}{dt} = 1.5\left(i_\alpha\dfrac{du_{g\alpha}}{dt} + u_{g\alpha}\dfrac{di_\alpha}{dt} + i_\beta\dfrac{du_{g\beta}}{dt} + u_{g\beta}\dfrac{di_\beta}{dt}\right) \\ \dfrac{dQ_{cl}}{dt} = 1.5\left(i_\alpha\dfrac{du_{g\beta}}{dt} + u_{g\beta}\dfrac{di_\alpha}{dt} - i_\beta\dfrac{du_{g\alpha}}{dt} - u_{g\alpha}\dfrac{di_\beta}{dt}\right) \end{cases} \tag{13}$$

During network unbalance, the positive and negative sequence voltages/currents can be expressed as (1).

Based on (2), the respective variation of α- and β-axis voltage, containing both positive and negative sequence components, can be obtained as,

$$\frac{du_{g\alpha}}{dt} = -\omega u'_{g\alpha} \quad \frac{du_{g\beta}}{dt} = -\omega u'_{g\beta} \tag{14}$$

Submitting (4), (12) and (14) to (13), equation (15) is obtained as,

$$\begin{cases} \dfrac{dP_{cl}}{dt} = -\dfrac{R}{L}P_{cl} - \omega Q_{ex} - \dfrac{3}{2L}\left(v_P - U_g^2\right) \\ \dfrac{dQ_{cl}}{dt} = \omega P_{ex} - \dfrac{R}{L}Q_{cl} - \dfrac{3}{2L}v_Q \end{cases} \tag{15}$$

where U_g is the grid voltage amplitude,

$$\begin{bmatrix} v_P \\ v_Q \end{bmatrix} = \begin{bmatrix} u_{g\alpha} & u_{g\beta} \\ u_{g\beta} & -u_{g\alpha} \end{bmatrix}\begin{bmatrix} v_\alpha \\ v_\beta \end{bmatrix} \tag{16}$$

As seen, through regulating the active and reactive powers, the modulated voltage v_P and v_Q respective for active and reactive powers can be simply produced as,

$$\begin{bmatrix} v_P \\ v_Q \end{bmatrix} = \begin{bmatrix} e_P \\ e_Q \end{bmatrix} - \frac{2}{3}L\begin{bmatrix} v'_P \\ v'_Q \end{bmatrix} \tag{17}$$

where G(s) is a transfer function of power controller, P_{fb} and Q_{fb} are the feedback powers,

$$\begin{bmatrix} v'_P \\ v'_Q \end{bmatrix} = \frac{d}{dt}\begin{bmatrix} P_{cl} \\ Q_{cl} \end{bmatrix} = G(s)\begin{bmatrix} P_{ref} - P_{fb} \\ Q_{ref} - Q_{fb} \end{bmatrix} \tag{18}$$

$$\begin{bmatrix} e_P \\ e_Q \end{bmatrix} = \begin{bmatrix} U_g^2 \\ 0 \end{bmatrix} - \frac{2R}{3}\begin{bmatrix} 1 & 0 \\ 0 & 1 \end{bmatrix}\begin{bmatrix} P_{cl} \\ Q_{cl} \end{bmatrix} + \frac{2\omega L}{3}\begin{bmatrix} 0 & -1 \\ 1 & 0 \end{bmatrix}\begin{bmatrix} P_{ex} \\ Q_{ex} \end{bmatrix} \tag{19}$$

Based on the inverse of (16), the VSI modulated voltage in the stationary reference frame can be deduced from the modulated voltage v_P and v_Q and calculated as,

$$\begin{bmatrix} v_\alpha \\ v_\beta \end{bmatrix} = \frac{1}{U_g^2}\begin{bmatrix} u_{g\alpha} & u_{g\beta} \\ u_{g\beta} & -u_{g\alpha} \end{bmatrix}\begin{bmatrix} v_P \\ v_Q \end{bmatrix} \tag{20}$$

Consequently, the modulated voltages can be produced by regulating the active and reactive powers in the stationary reference frame without PLL and Park Transformations. However, based on (4), the active and reactive powers contain both the average part and the oscillating part with unbalanced current provision. It is necessary to address the flexible power regulation for a trade-off between the power oscillation and the current unbalance. Meanwhile, under grid faults, the initial power reference cannot be achieved due to the current safety value. Consequently, a power limiter needs to be introduced for keeping the currents under the pre-defined threshold and operating for better utilization of the inverter power capacity. Thus, the flexible power regulation and limitation need to be developed for achieving the trade-off operation between the power oscillations and the current unbalance and avoiding the overcurrent tripping under unbalanced faults.

III. Control System

A. Power Regulation

This part is focused on the flexible power regulation of the power oscillation and the current unbalance under unbalanced faults. Instead of adding the specific power compensations to the power reference, this paper develops the flexible power

feedbacks through combining the classical and extended power theory. In this method, the feedback powers are reconstructed with an adjustable parameter λ. For the average power tracking, the coefficients of the extended and classical powers are designed to be added to one. Then, the adjustable parameter is between 0 and 1, i.e., $\lambda\in[0,1]$. Thus, the flexible power feedbacks are designed as,

$$\begin{cases} P_{\rm fb} = \lambda P_{\rm ex} + (1-\lambda) P_{\rm cl} \\ Q_{\rm fb} = (1-\lambda) Q_{ex} + \lambda Q_{\rm cl} \end{cases} \tag{21}$$

Based on the previous analysis, the feedback powers consist of both dc parts and oscillating parts at twice the grid frequency. The power controller is capable of not only regulating dc signals but also nullifying the oscillating signals at twice the grid frequency. Consequently, a PIR controller with a cutoff frequency is used in (18) and expressed as,

$$G(s)=k_{\rm p}+\frac{k_{\rm i}}{s}+\frac{k_{\rm r}\omega_{\rm c}s}{s^2+\omega_{\rm c}s+4\omega^2} \tag{22}$$

Since PIR controller can eliminate the steady-state errors at twice the grid frequency, the oscillating powers are controlled to be zero with specific negative sequence currents. Therefore, the following equations can be obtained by,

$$\begin{cases} P_{\rm cli2}+(1-2\lambda)P_{\rm clu2}=0 \\ Q_{\rm cli2}-(1-2\lambda)Q_{\rm clu2}=0 \end{cases} \tag{23}$$

Submitting (5) and (6) into (23), the amplitude and phase angle of negative sequence currents with an adjustable parameter λ can be obtained by,

$$\begin{cases} I_{-}=(1-2\lambda)U_{\rm g-}I_{+}/U_{\rm g+} \\ \theta_{i-}=\theta_{\rm u+}-\theta_{i+}+\theta_{\rm u-}+\pi \end{cases} \quad (0\le\lambda<0.5) \tag{24}$$

$$\begin{cases} I_{-}=(2\lambda-1)U_{\rm g-}I_{+}/U_{\rm g+} \\ \theta_{i-}=\theta_{\rm u+}-\theta_{i+}+\theta_{\rm u-} \end{cases} \quad (0.5<\lambda\le1) \tag{25}$$

It is seen that the oscillating parts of feedback power at twice the grid frequency in (21) can be eliminated only with negative sequence currents injected, whose amplitude and phase angle are specified with an adjustable parameter λ in (23). In other words, it only needs the injection of proper negative sequence currents but not 3rd-order harmonic currents. Consequently, VSI currents remain highly sinusoidal under unbalanced faults.

According to (5), (6) and (23), the amplitudes of the oscillating classical active and reactive powers are obtained as,

$$\begin{cases} P_{\rm cl2}=P_{\rm cli2}+P_{\rm clu2}=3\lambda U_{\rm g-}I_{+}\cos(-2\omega t+\theta_{\rm u-}-\theta_{\rm i+}) \\ Q_{\rm cl2}=Q_{\rm cli2}+Q_{\rm clu2}=3(1-\lambda)U_{\rm g-}I_{+}\sin(-2\omega t+\theta_{\rm u-}-\theta_{\rm i+}) \end{cases} \tag{26}$$

Single-phase voltage sag is the commonest type of grid fault and accounts for 70-85% [16], [17]. Thus, a single-phase sag, e.g., the sag of phase A, is taken as an example representing asymmetrical faults in the following analysis. The voltage sag in phase A is recorded as $u'_{\rm ga}=k\cdot u_{\rm ga}$ (k is the drop depth), while the voltages in phase B, C remain nominal. As analyzed in [19], with the symmetrical component method, the per-unit amplitudes of positive and negative sequence voltages are expressed as,

$$\begin{cases} U_{\rm g+}=(2+k)/3 \\ U_{\rm g-}=(1-k)/3 \end{cases} \tag{27}$$

Since negative-sequence powers produced by negative-sequence voltages and currents are relatively small, they are nearly neglected. For simple analysis, the product of the amplitudes of the positive sequence voltage and current can be nearly regarded as the apparent power. Thus, the per-unit amplitude of positive sequence current is obtained by,

$$I_{+}=\frac{3}{2+k}S \tag{28}$$

where S is the per-unit value of the apparent power.

According to (23)-(27), the amplitudes of negative sequence currents and oscillating amplitude of classical active/reactive powers can be expressed as,

$$\begin{cases} I_{-}=3\left|1-2\lambda\right|(1-k)/(2+k)^2\times S \\ P_{\rm cl2m}=3\lambda(1-k)/(2+k)\times S \\ Q_{\rm cl2m}=3(1-\lambda)(1-k)/(2+k)\times S \end{cases} \tag{29}$$

where $P_{\rm cl2m}$ and $Q_{\rm cl2m}$ are the amplitudes of the oscillating active and reactive powers, respectively.

As seen from Fig. 2, with an adjustable parameter λ, the amplitudes of the negative sequence currents and the oscillating active and reactive powers can be flexible regulated. A trade-off between the negative sequence current and the oscillating power is achieved. In particular, the special conditions of the control strategy can be divided into four modes as shown in Table I.

TABLE I
CONTROL MODES OF POWER REGULATION

Scheme	Operation Targets	λ
Mode I	Constant active power	0
Mode II	Balance sinusoidal current	0.5
Mode III	Constant reactive power	1
Mode IV	Flexible power regulation	[0,1]

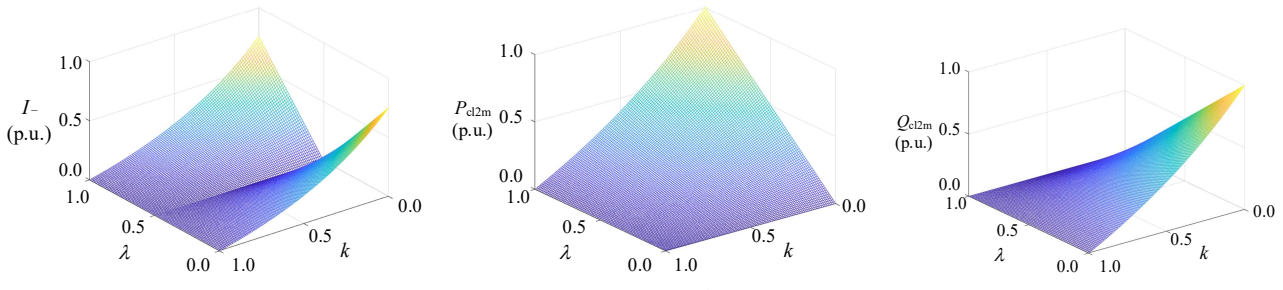

Fig. 2 Plots with variable parameter λ and drop depth k at S=1.0: (a) amplitude of negative sequence current; (b) amplitude of oscillating active power; (c) amplitude of oscillating reactive power.

B. Power Limitation

As seen from (28), the current would exceed the limited threshold due to the voltage dip for the initial power delivery. Then, the overcurrent tripping and disconnection arise. Thus, together with the flexible power regulator, a power limiter must be designed and applied to limit the apparent power under unbalanced faults so that the inverter remains connected to the grid.

With the predefined current threshold, the apparent power of the converter must be updated in real-time based on various voltages. It is called new apparent power (NAP). Normally, NAP is less than the rated power of the converter, which depends on the voltage sag. As analyzed, the peak currents are determined not only by the apparent power but also the coupling active-reactive power. If the converter operates at unity or zero power factor without the coupling terms, the apparent power in unity power factor (or zero power factor) mode is minimum. Thus, to be conservative, the minimum value of the active power in unity power factor mode and the reactive power in zero factor mode can be set as NAP. Thus, NAP is achieved by,

$$NAP = \min\left(P_{\mathrm{cl0}}\left|_{\theta_{\mathrm{u}+}-\theta_{i+}=0}, Q_{\mathrm{cl0}}\right|_{\theta_{\mathrm{u}+}-\theta_{i+}=\pi/2}\right) \tag{30}$$

where

$$\begin{cases} P_{\mathrm{cl0}} = 1.5U_{\mathrm{g}+}I_{+} + 1.5U_{\mathrm{g}-}I_{-} = 1.5U_{\mathrm{g}+}I_{+}\left[1-\left(1-2\lambda\right)k_{\mathrm{pn}}^{2}\right] \\ Q_{\mathrm{cl0}} = 1.5U_{\mathrm{g}+}I_{+} + 1.5U_{\mathrm{g}-}I_{-} = 1.5U_{\mathrm{g}+}I_{+}\left[1+\left(1-2\lambda\right)k_{\mathrm{pn}}^{2}\right] \end{cases} \tag{31}$$

where $k_{\mathrm{pn}} = U_{\mathrm{g}-}/U_{\mathrm{g}+}$ is the voltage unbalance factor.

$$k_{\mathrm{pn}} = \frac{1-k}{2+k} \tag{32}$$

Accordingly, (30) can be simplified as,

$$NAP = 1.5U_{\mathrm{g}+}I_{+}\left[1-\left|1-2\lambda\right|k_{\mathrm{pn}}^{2}\right] \tag{33}$$

The maximum current vector arises when the positive and the negative sequence current vectors are in the same direction. If the maximum current vector is coincided with A (or B, C) axis, the peak current value in phase A (or B, C) is equal to the amplitude of the current vector. Then, the maximum current value can be calculated as,

$$I_{\max} = I_{+} + I_{-} = \left(1+\left|1-2\lambda\right|k_{\mathrm{pn}}\right)I_{+} \le I_{\mathrm{th}} \tag{34}$$

where $I_{\max}$ is the maximum amplitude of current vector, I_{th} is the per-unit value of the safe current threshold.

According to (28), (33) and (34), the maximum NAP is obtained as,

$$S_{\mathrm{th}} = \frac{\left(2+k\right)\left[1-\left|1-2\lambda\right|k_{\mathrm{pn}}^{2}\right]}{2\left[1+\left|1-2\lambda\right|k_{\mathrm{pn}}\right]}I_{\mathrm{th}} \tag{35}$$

where S_{th} is the maximum apparent power.

It is noted that the angle of the maximum current vector varies between 0 and 2π, which may not be coincided with A (or B, C) axis. Under such case, the peak phase current value is less than the amplitude of current vector due to the vector projection. Consequently, S_{th} is a relatively conserved value.

Fig. 3 illustrates the impact of variable parameter λ and drop depth k on the maximum apparent power S_{th}. It is assumed that the per-unit value of the safe current threshold is 1.0 p.u.. It is

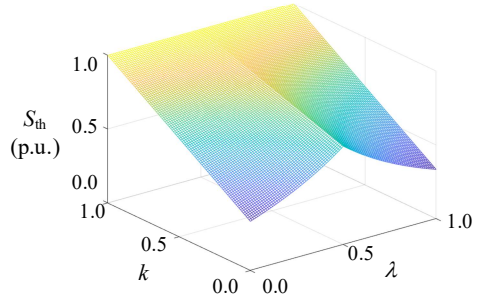

Fig. 3 Plots of maximum apparent power with variable parameter λ and drop depth k at I_{th}=1.0.

demonstrated that the voltage drop will result in the reduction of NAP. For a certain drop depth, NAP varies with the variable parameter λ. The maximum apparent power S_{th} arrives at the maximum value at λ=0.5, while it reaches the minimum valueat λ=0.0 and 1.0. It means that for delivering more powers, Mode II, i.e., balanced sinusoidal currents, is suggested under voltage sags.

C. System Implementation

During voltage faults, inverters are required to provide grid-supporting functionalities, especially injection of the capacitive reactive power. The reactive power is calculated as,

$$Q_{\mathrm{ref}} = \begin{cases} 0 & \left(U_{\mathrm{g}+} > 0.9\right) \\ k_{\mathrm{Q}}Q_{\max}\left(1-U_{\mathrm{g}+}\right) & \left(1-1/k_{\mathrm{Q}} < U_{\mathrm{g}+} < 0.9\right) \\ Q_{\max} & \left(U_{\mathrm{g}+} < 1-1/k_{\mathrm{Q}}\right) \end{cases} \tag{36}$$

where $Q_{\max}$ is the maximum output reactive power at $U_{\mathrm{g}+}$, k_{Q} is the proportional parameter which is initially set to be two if not otherwise specified. When $U_{\mathrm{g}+}$ drops below 0.9 p.u., as the reactive power requirement enforced by Danish Grid Code in [23], the inverter should provide 2% reactive power for every 1% voltage deviation. Since the reactive power is prioritized over the active power during voltage sags, the full inverter capacity would be assigned to reactive power under severe conditions. In other words, the maximum reactive power provided by inverters in (36) is set as the maximum apparent power, i.e., $Q_{\max} = S_{\mathrm{th}}$. Then, based on the maximum apparent power in (35) and Q_{ref} in (36), the maximum allowed active power with current constraints is achieved as,

$$P_{\max} = \sqrt{S_{\mathrm{th}}^{2} - Q_{\mathrm{ref}}^{2}} \tag{37}$$

During voltage sags, $P_{\max}$ is always compared to the initial reference power P_{ref0}. If $P_{\max} > P_{\mathrm{ref0}}$, the amount of active power injected into the grid before sag can be still delivered. If $P_{\max} < P_{\mathrm{ref0}}$, the inverter cannot inject the commanded active power due to power limitation. Thus, the active power reference in (18) can be obtained by,

$$P_{\mathrm{ref}} = \begin{cases} P_{\mathrm{ref0}} & \left(P_{\mathrm{ref0}} < P_{\max}\right) \\ P_{\max} & \left(P_{\mathrm{ref0}} > P_{\max}\right) \end{cases} \tag{38}$$

Fig. 4 gives the diagram of the power limitation so as to facilitate understanding. In Fig. 4, P_{ref0} is the initial active power reference, while P_{ref} represents the active power reference with the power limitation. Firstly, during grid fault, together with the grid requirement, Q_{ref} is determined based on

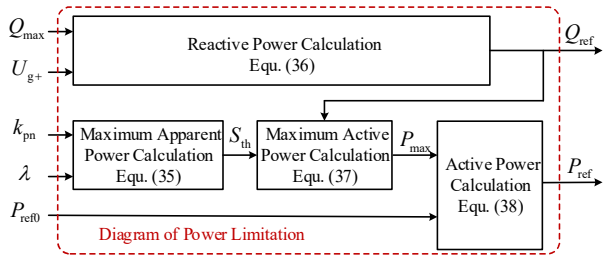

Fig. 4 The calculation flow chart of power limitation.

the positive voltage and the maximum reactive power Q_{max} according (36). Meanwhile, in (35), the maximum apparent power S_{th} is calculated with voltage unbalance factor k_{pn} and the adjustable parameter λ determined by the external requirements. Then, the available active power P_{max} is obtained based on (37). Finally, together with the initial active power reference, the commanded value of the active power, being the smaller one between P_{ref0} and P_{max}, is given in (38). Except for the inverter capacity for the reactive power provision, the surplus capacity is fully utilized for the active power delivery.

Fig. 5 gives the proposed control block diagram for flexible power regulation and limitation. Since the calculation of the delayed voltage and positive/negative sequence voltage amplitude is not in the scope of this paper, the voltage vector is simply delayed by $T/4$, where T = 20 ms is the fundamental period. The amplitudes of positive and negative sequence voltages are obtained with $T/4$ delayed signal cancellation method. Then, the active and reactive power references are calculated with the positive and negative sequence voltages and the adjustable parameter λ through power limitation which is shown in Fig. 4. PIR controllers are used to regulating the power feedbacks, thereby resulting in a flexible power regulation without any power compensation. Then, the modulated voltage v_P and v_Q respective for active and reactive powers can be produced by (17). Finally, with the modulated given in (20), the SVM technique is introduced to produce the required switching voltage vectors with their duration time.

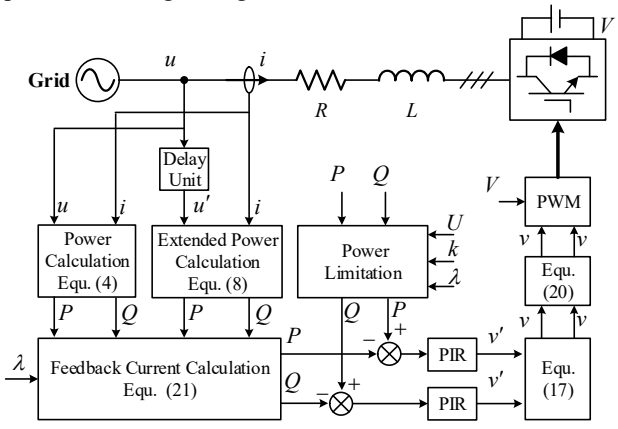

Fig. 5 Proposed control block diagram.

IV. Hardware-in-loop Tests

To validate the proposed power regulation and limitation, the corresponding hardware-in-loop (HIL) tests are conducted using RTLAB OP5700 and NI PXIe-1071. The equipment of the HIL test is given in Fig. 6, where the main loop shown in Fig. 1 is simulated in RTLAB and the control algorithm is

TABLE II
System Parameters

Parameters	Values	Parameters	Values
Rated power	200 kW	Rated voltage	310 V
ω	100π rad/s	DC voltage	600 V
L	2.0 mH	R	0.01 Ω

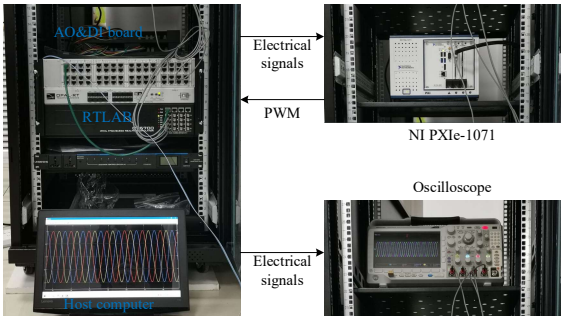

Fig. 6 HIL test setup.

realized through the NI PXIe-1071. The rated parameters are listed in Table II. All the waveforms are acquired by an Tektronix MDO3024 scope.

Fig. 7 gives the VSI performance under one single-phase grid fault, in which u_{ga} falls to 0.5 p.u.. Under such a case, the commanded reactive power is set at 0.35 p.u., while the commanded active power remains 1.0 p.u. due to no current limitation. As seen, during the grid fault, the converter current remains highly sinusoidal with its total harmonic distortion (THD) being 1.4%. Then, as with the increasing adjustable parameter λ from 0 to 1, the negative sequence current is flexibly controlled for achieving different power behaviors. It is observed that both the active and reactive powers can be regulated in a flexible way for some specific applications which are sensitive to power oscillations. Under such a case, since the positive sequence voltage falls to 0.83 p.u., for maintaining the rated power delivery, the converter current will increase, which is larger than the rated value all the time. The over-current

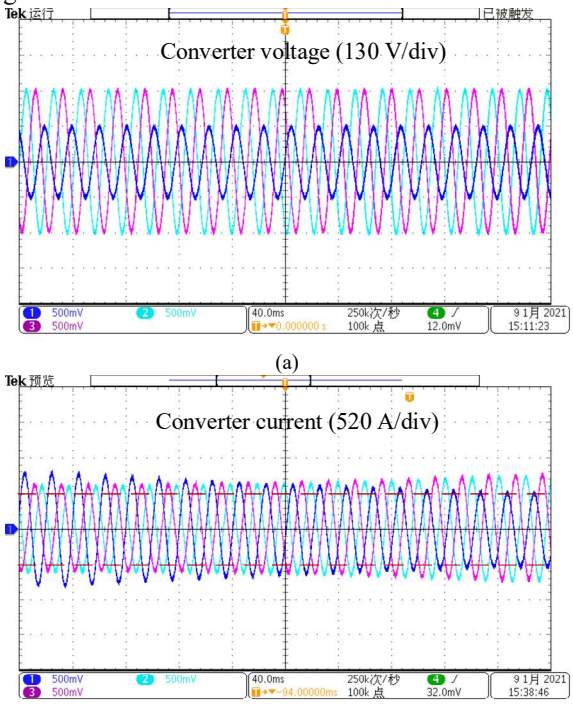

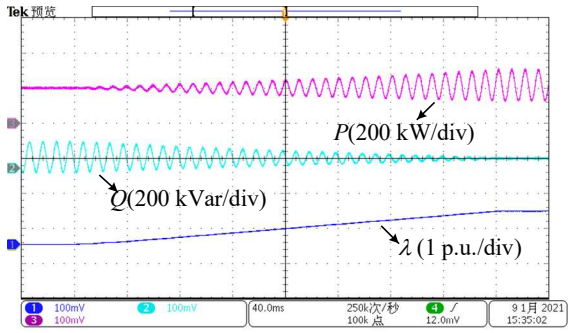

(c)

Fig. 7 Results of converter current and power under a single-phase fault without power limiter. (a) grid voltage (40ms/div); (b) inverter current (40ms/div); (c) inverter active and reactive power (40ms/div).

phenomenon under the single-phase grid fault rises, which is expected to be avoided.

Fig. 8 gives the converter currents and active/reactive powers under one single-phase grid fault. The grid voltage condition is the same as that in Fig. 7. Since the reactive power is in the priority under grid fault, the commanded reactive power is set at 0.35 p.u.. Then, based on (35), it is noted that the maximum value of the NAP is relevant to the adjustable parameter λ. As λ = 0.5, the NAP reaches its maximum value 0.83 p.u., while it decreases to 0.67 p.u. at λ = 0 or 1.0. Thus, the average active power would change with the increasing adjustable parameter λ from 0 to 1. It can be seen from Fig. 8(b) that when the power limitation control strategy is implemented, the average value of the active power first rises and then falls. When λ = 0.5 at t = 200ms, the average active power arrives at its maximum value, as shown in Fig. 8, which is consistent with the theoretical analysis in Fig. 3. As seen, by enabling the power limiter in (37), the converter current is always limited at a pre-defined threshold under the unbalanced grid faults. In other words, the power limiter avoids the over-current phenomenon under the single-phase grid fault. Besides, the negative sequence currents are also flexibly regulated for the achievement of the oscillating power mitigation.

Fig. 9 gives the dynamic performance of the converter under a single-phase voltage sag in which u_{ga} falls to 0.5 p.u. at 60 ms. In the tests, the active and reactive powers are initially set at 1.0 and 0.0 p.u., respectively. The adjustable parameter λ is fixed at 0.5 for removing the negative sequence current and guaranteeing a balanced current. Under such a case, the reactive power reference is obtained as 0.35 p.u., while based on (37), the active power reference is calculated as 0.75 p.u.,

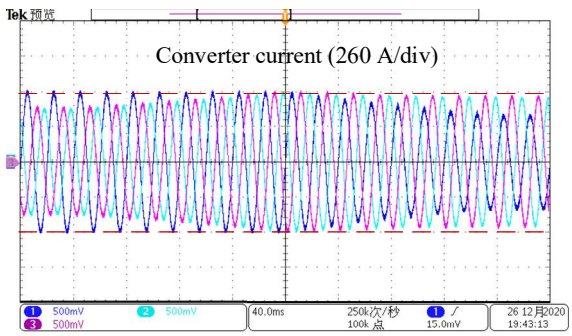

(a)

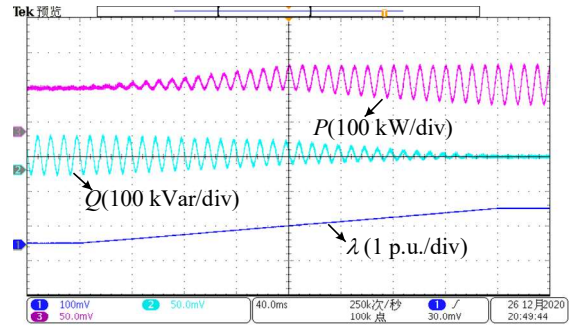

(b)

Fig. 8 Results of converter current and power under a single-phase fault with power limiter. (a) converter current (40ms/div); (b) converter active and reactive power (40ms/div).

respectively. The VSI current remains highly sinusoidal with its THD being 1.5% under the single-phase voltage sag. The converter current is controlled to be balanced without the negative sequence components as required. Since the power limiter is enabled, the converter current of each phase is always limited at the rated value under asymmetrical voltage conditions, which avoids the over-current phenomenon under the single-phase voltage sag. Due to the interaction between the positive sequence current and the negative sequence voltage, the power oscillations are inevitable under such a case.

Fig. 10 gives the dynamic performance of the converter under a two-phase voltage sag in which u_{ga} and u_{gb} falls to 0.5 p.u. at 60 ms. In the tests, the active and reactive powers are initially set at 1.0 and 0.0 p.u., respectively. The adjustable parameter λ is fixed at 0.5 for removing the negative sequence current. It is seen that the converter currents are balanced with its THD being around 1.5%. During the two-phase voltage sag, the converter current is always under the pre-defined threshold without the over-current phenomenon.

Consequently, based on the aforementioned HIL test results, it can be concluded that the proposed power control strategy

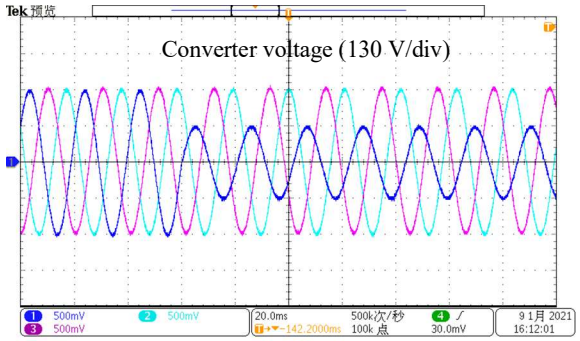

(a)

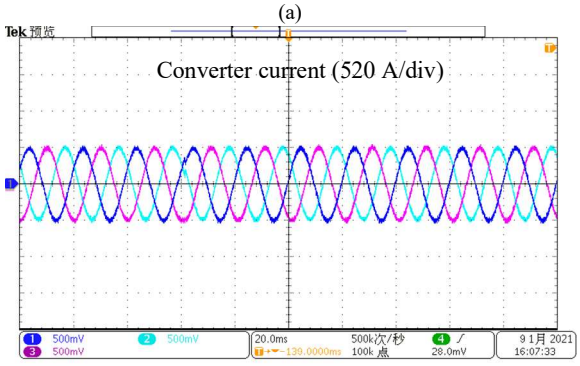

(b)

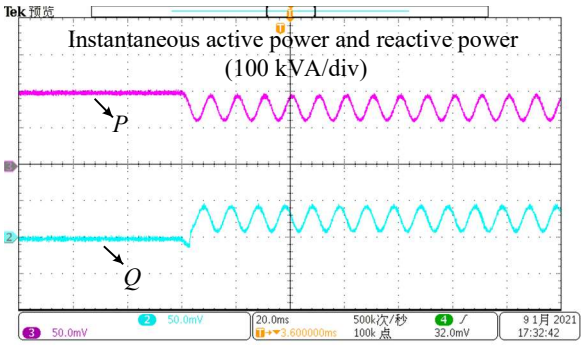

(c)

Fig. 9 Dynamic performance under a single-phase voltage fault. (a) grid voltage (20ms/div); (b) converter current (20ms/div); (c) converter active and reactive power (20ms/div).

can provide both satisfactory steady-state performance and well dynamic responses under unbalanced faults. Meanwhile, the proposed method is more suitable for a VSI to regulate its power oscillations in a flexible way for some specific applications under unbalanced faults.

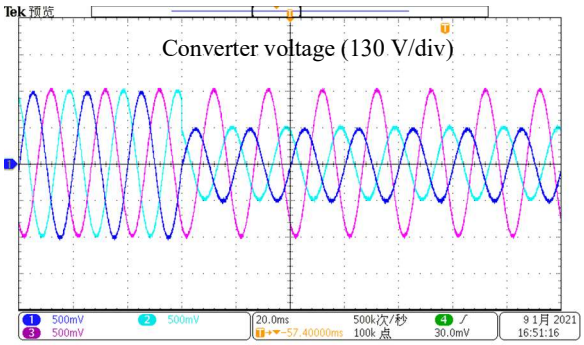

(a)

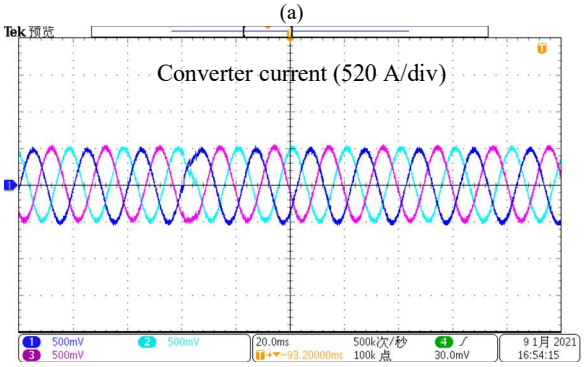

(b)

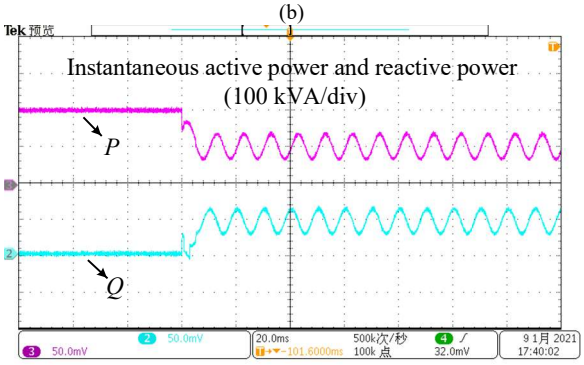

(c)

Fig. 10 Dynamic performance under a two-phase voltage fault. (a) grid voltage (20ms/div); (b) converter current (20ms/div); (c) converter active and reactive power (20ms/div).

V. Conclusion

This paper develops a flexible power regulation and limitation of a VSI under unbalanced faults. By combing the classical and extended power theory, the flexible power feedbacks are fully designed with an adjustable parameter as required for the achievement of the trade-off between the current unbalance and the power oscillations. Then, the available NAP is calculated on the basis of the adjustable parameter and the voltage drop depth. Together with the available NAP, a power limiter is developed under unbalanced faults, which can keep the currents under the pre-defined threshold and operate for better utilization of the inverter power capacity under unbalanced grid faults. Thus, the VSI can avoid overcurrent tripping while flexibly regulating the power behaviors under unbalanced grid faults. All the calculations and implementations are carried out in the stationary reference frame without the need of the PLL. The real-time HIL tests also verify that the proposed flexible power regulation and limitation can provide both satisfactory steady-state behaviors and dynamic responses.

References

[1] F. Blaabjerg, Y. H. Yang, D. S. Yang, and X. F. Wang, "Distributed power-generation systems and protection," *Proceedings of the IEEE*, vol. 105, no. 7, pp. 1311-1331, Jul, 2017.

[2] F. Blaabjerg, and K. Ma, "Wind energy systems," *Proceedings of the IEEE*, vol. 105, no. 11, pp. 2116-2131, Nov, 2017.

[3] S. D'Arco, L. Piegari, and P. Tricoli, "Comparative analysis of topologies to integrate photovoltaic sources in the feeder stations of AC railways," *IEEE Trans. Transport. Electrific.*, vol. 4, no. 4, pp. 951-960, Dec, 2018.

[4] S. Golestan, J. M. Guerrero, and J. C. Vasquez, "Three-phase PLLs: A review of recent advances," *IEEE Trans. Power Electron.*, vol. 32, no. 3, pp. 1897-1907, Mar, 2017.

[5] J. Jia, G. Yang, and A. H. Nielsen, "A Review on grid-connected converter control for short-circuit power provision under grid unbalanced faults," *IEEE Trans. Power Del.*, vol. 33, no. 2, pp. 649-661, Apr, 2018.

[6] S. F. Zarei, H. Mokhtari, M. A. Ghasemi, S. Peyghami, P. Davari, and F. Blaabjerg, "Control of grid-following inverters under unbalanced grid conditions," *IEEE Trans. Energy Convers.*, vol. 35, no. 1, pp. 184-192, Jan, 2019.

[7] J. Eloy-Garcia, S. Arnaltes, J.L. Rodriguez-Amenedo, "Direct power control of voltage source inverters with unbalanced grid voltages," *IET Power Electronics*, vol. 1, no. 3, pp. 395-407, Sep, 2008.

[8] G. Escobar, A. M. Stankovic, J. M. Carrasco, E. Galvan and R. Ortega, "Analysis and design of direct power control (dpc) for a three phase synchronous rectifier via output regulation subspaces," *IEEE Transactions on Power Electronics*, vol. 18, no. 3, pp. 823-830, May, 2003.

[9] D. Zhou, P. Tu, and Y. Tang, "Multivector model predictive power control of three-phase rectifiers with reduced power ripples under nonideal grid conditions," *IEEE Trans. Ind. Electron.*, vol. 65, no. 9, pp. 6850-6859, Sep, 2018.

[10] Y. C. Zhang, C. Q. Qu, and J. H. Gao, "Performance improvement of direct power control of PWM rectifier under unbalanced network," *IEEE Trans. Power Electron.*, vol. 32, no. 3, pp. 2319-2328, Mar, 2017.

[11] H. Nian, Y. Shen, H. Yang, and Y. Quan, "Flexible grid connection technique of voltage-source inverter under unbalanced grid conditions based on direct power control," *IEEE Trans. Ind. Appl.*, vol. 51, no. 5, pp. 4041-4050, Sep-Oct, 2015.

[12] D. Sun, X. Wang, H. Nian, and z. q. zhu, "A sliding-mode direct power control strategy for DFIG under both balanced and unbalanced grid conditions using extended active power," *IEEE Trans. Power Electron.*, vol. 33, no. 2, pp. 1313-1322, Feb, 2017.

[13] Y. H. Gui, C. Kim, C. C. Chung, J. M. Guerrero, Y. J. Guan, and J. C. Vasquez, "Improved direct power control for grid-connected voltage source converters," *IEEE Trans. Ind. Electron.*, vol. 65, no. 10, pp.

8041-8051, Oct, 2018.

[14] Y. H. Gui, M. S. Li, J. H. Lu, S. Golestan, J. M. Guerrero, and J. C. Vasquez, "A Voltage modulated DPC approach for three-phase PWM rectifier," *IEEE Trans. Ind. Electron.*, vol. 65, no. 10, pp. 7612-7619, Oct, 2018.

[15] S. Gao, H. Zhao, Y. Gui, D. Zhou, V. Terzija, and F. Blaabjerg, "A Novel Direct Power Control for DFIG with Parallel Compensator under Unbalanced Grid," *IEEE Trans. Ind. Electron.*, vol. 68, no. 10, pp. 9607-9618, Oct. 2021.

[16] H. D. Tafti, A. I. Maswood, G. Konstantinou, J. Pou, and P. Acuna, "Active/reactive power control of photovoltaic grid-tied inverters with peak current limitation and zero active power oscillation during unbalanced voltage sags," *IET Power Electron.*, vol. 11, no. 6, pp. 1066-1073, Jun, 2018.

[17] B. Mahamedi, M. Eskandari, J. E. Fletcher, and J. Zhu, "Sequence-based control strategy with current limiting for the fault ride-through of inverter-interfaced distributed generators," *IEEE Trans. Sustain. Energy*, vol. 11, no. 1, pp. 165-174, Jan, 2020.

[18] X. Q. Guo, W. Z. Liu, and Z. G. Lu, "Flexible power regulation and current-limited control of the grid-connected inverter under unbalanced grid voltage faults," *IEEE Trans. Ind. Electron.*, vol. 64, no. 9, pp. 7425-7432, Sep, 2017.

[19] Z. Shuai, M. Xiao, J. Ge, and Z. J. Shen, "Overcurrent and its restraining method of PQ-controlled three-phase four-wire converter under asymmetrical grid fault," *IEEE J. Emerg. Sel. Topics Power Electron.*, vol. 7, no. 3, pp. 2057-2069, Mar, 2019.

[20] A. Camacho, M. Castilla, J. Miret, A. Borrell, and L. G. De Vicuña, "Active and reactive power strategies with peak current limitation for distributed generation inverters during unbalanced grid faults," *IEEE Trans. Ind. Electron.*, vol. 62, no. 3, pp. 1515-1525, Mar, 2015.

[21] E. Afshari, G. R. Moradi, R. Rahimi, B. Farhangi, Y. Yang, F. Blaabjerg, and S. Farhangi, "Control strategy for three-phase grid-connected PV inverters enabling current limitation under unbalanced faults," *IEEE Trans. Ind. Electron.*, vol. 64, no. 11, pp. 8908-8918, Nov, 2017.

[22] M. G. Taul, X. F. Wang, P. Davari, and F. Blaabjerg, "Current reference generation based on next-generation grid code requirements of grid-tied converters during asymmetrical faults," *IEEE J. Emerg. Sel. Top. Power Electron.*, vol. 8, no. 4, pp. 3784-3797, Dec, 2020.

[23] Mohseni M, Islam S M, "Review of international grid codes for wind power integration: diversity, technology and a case for global standard," *Renewable and Sustainable Energy Reviews*, vol. 16, no. 6, pp. 3876-3890, Aug, 2012.

Peng Cheng was born in Liaoning Province, China. He received the B.S. and Ph.D. degree from Zhejiang University, Hangzhou, China, in 2011 and 2016, both in electrical engineering. He is currently an assistant professor in the Department of China Institute of Energy and Transport Integration Development, North China Electric Power University, China.

His current research interests include multi-converter power systems and renewable power generation, particularly wind power generation.

Kongyuan Li was born in Guangdong Province, China. He received the B.S. degree in electrical engineering from North China Electric Power University, Beijing, China, in 2020. He is currently working toward the M.S. degree in North China Electric Power University, Beijing, China.

His current research interests include multi-converter power systems and the transient stability of power converters.

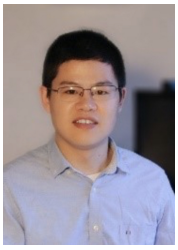

Chao Wu (M'19) was born in Hubei Province, China. He received the B.Eng. degree from HeFei University of Technology, Hefei, China and the Ph.D. degree from Zhejiang University, Hangzhou, China, in 2014 and 2019, both in electrical engineering. From 2019 to 2021, he was a Postdoctoral Researcher in the Department of Energy Technology, Aalborg University, Aalborg, Denmark. He is currently an assistant professor in the Department of Electrical Engineering, Shanghai JiaoTong University, Shanghai, China.

His current research interests include modeling, control, and stability analysis of power electronics in renewable energy applications, particularly the control and operation of doubly fed induction generators for DC connection and the transient stability of power converters. He has published more than 20 IEEE/IET Transaction papers.

Jing Ma received his B.S. and Ph.D. degree from North China Electric Power University, China, in 2003 and 2008, respectively. He has been a visiting research scholar in the Bradley Department of Electrical and Computer Engineering, Virginia Polytechnic Institute and State University from 2008 to 2009. He is currently a professor in the School of Electrical and Electronic Engineering, North China Electric Power University, China. His major interests include power system stability and control.

Limin Jia received the Ph.D. degree in the Automation and Control in Transportation from the China Academy of Railway Sciences, Beijing, China, in 1991. He is currently a Professor with North China Electric Power University and with Beijing Jiaotong University, where he is Head of China Institute of Energy and Transport Integrated Development and Chief Scientist of the National Center of Collaborative Innovation Center for Rail Safety and the State Key Laboratory of Rail Traffic Control and Safety. He is a member of the first batch of Millions of Leading Engineering Talents Project. His research interests include the integrated development of energy and transportation, the intelligent transportation, and the rail traffic control.